

The Electric Field Induced in the Brain by Magnetic Stimulation: A 3-D Finite-Element Analysis of the Effect of Tissue Heterogeneity and Anisotropy

Pedro C. Miranda*, Mark Hallett, and Peter J. Basser

Abstract—We investigate the effect of tissue heterogeneity and anisotropy on the electric field and current density distribution induced in the brain during magnetic stimulation. Validation of the finite-element (FE) calculations in a homogeneous isotropic sphere showed that the magnitude of the total electric field can be calculated to within an error of approximately 5% in the region of interest, even in the presence of a significant surface charge contribution. We used a high conductivity inclusion within a sphere of lower conductivity to simulate a lesion due to an infarct. Its effect is to increase the electric field induced in the surrounding low conductivity region. This boost is greatest in the vicinity of interfaces that lie perpendicular to the current flow. For physiological values of the conductivity distribution, it can reach a factor of 1.6 and extend many millimeters from the interface. We also show that anisotropy can significantly alter the electric field and current density distributions. Either heterogeneity or anisotropy can introduce a radial electric field component, not present in a homogeneous isotropic conductor. Heterogeneity and anisotropy are predicted to significantly affect the distribution of the electric field induced in the brain. It is, therefore, expected that anatomically faithful FE models of individual brains which incorporate conductivity tensor data derived from diffusion tensor measurements, will provide a better understanding of the location of possible stimulation sites in the brain.

Index Terms—Anisotropic media, brain, conductivity, current density, eddy currents, electric fields, electromagnetic induction, finite element methods, magnetic stimulation, nonhomogeneous media.

I. INTRODUCTION

MAGNETIC stimulation, a technique based on the principle of electromagnetic induction, is used to excite tissue in the human nervous system painlessly and noninvasively [1]–[3]. Transcranial magnetic stimulation (TMS) is used routinely to test the central motor pathways [4]. It is also a research tool for investigating brain physiology and function [4], [5] as well as cognition [6], [7]. It may also prove helpful in the treatment of psychiatric diseases such as depression [8].

Manuscript received September 21, 2001; revised February 8, 2003. The work of P. C. Miranda was supported in part by a grant from the Calouste Gulbenkian Foundation, Portugal. *Asterisk indicates corresponding author.*

*P. C. Miranda is with the Institute of Biophysics and Biomedical Engineering, Faculty of Sciences, University of Lisbon, 1749-016 Lisbon, Portugal (e-mail: pmcm@fc.ul.pt).

M. Hallett is with the Human Motor Control Section, MNB, NINDS, National Institutes of Health, Bethesda, MD 20892-1428, USA (e-mail: hallettm@ninds.nih.gov).

P. J. Basser is with the Section on Tissue Biophysics & Biomimetics, LIMB, NICHD, National Institutes of Health, Bethesda, MD 20892-5772 USA.

Digital Object Identifier 10.1109/TBME.2003.816079

Despite the widespread and successful application of TMS, it is not possible to predict precisely the territory that is affected. Addressing this problem requires knowledge of the spatial distribution of the electric field induced within the head and the mechanism of interaction between the induced electric field and neural tissue.

The mechanism whereby brain tissues are stimulated is not yet completely understood. In the cortex, axons are often short compared with the dimension of the coil and follow bent paths. It has been demonstrated *in vitro* [9]–[11] and predicted theoretically [12] that regions where axons terminate, bend or branch represent low threshold points for stimulation. In such regions, activation is determined primarily by the strength of the component of the induced electric field parallel to the axon. This contrasts with the case of a long straight axon for which the activation function is dominated by the gradient of the induced electric field along the direction of the axon [10], [13]–[16]. Results obtained by TMS of the human visual cortex [17] and motor cortex [18]–[20] are consistent with stimulation occurring at the peak of the electric field rather than that of its gradient.

Making accurate calculations of the distribution of the electric field induced in the brain is difficult because tissue heterogeneity and anisotropy as well as head geometry must be taken into account. The surface charge that builds up on the air/tissue boundary to ensure that the current density normal to that surface is zero, significantly decreases the induced electric field within the conducting volume and markedly affects its spatial distribution [21], [22]. For example, Roth *et al.* [23], [24] calculated the electric field distribution induced in an idealized three-layer spherical model of the head for different coil configurations and positions, using a finite difference approximation. They showed that the spherical boundary distorts the electric field distribution and reduces its radial component to zero. Heterogeneity has also been shown to have a significant impact on the induced electric field distribution and on the location of the stimulation site [25], [26]. To the best of our knowledge, the effect of tissue anisotropy on the stimulation of the central nervous system has not been investigated.

A detailed knowledge of the electric field distribution, incorporating all of the effects mentioned above, is necessary to interpret the results of some TMS studies. For example, the presence of a high conductivity lesion resulting from a cortical stroke may increase the amplitude of the motor responses to TMS, independently of changes in the properties of the excitable tissue. TMS maps in the affected hemisphere are liable to be enlarged and displaced relative to the underlying responding tissue. Also,

changes in tissue conductivity may occur during recovery and confound longitudinal studies, particularly during the subacute phase.

The finite-element (FE) method [27] for solving partial differential equations is ideally suited to calculate the electric field distribution induced in heterogeneous, anisotropic tissues with complex boundaries. So far, it has been used by only a few authors to calculate induced current distributions in simple geometric models [28], [29] and in models of the dog's thorax [30] and the human brain [31].

To date, the biggest impediment to using the FE method has been the scarcity of anatomically accurate conductivity data. The recent development of diffusion tensor magnetic resonance imaging (DT-MRI) has enabled the localized measurement of the effective water self-diffusion tensor *in vivo* [32]. Information about the effective electrical conductivity tensor can be obtained from the diffusion tensor if the assumption is made that they both share the same set of eigenvectors [33]. A scheme for scaling the diffusion eigenvalues into conductivity eigenvalues has been proposed by Tuch *et al.* [34]. Thus, for the first time, DT-MRI could provide a noninvasive method for obtaining electrical conductivity tensor maps in individual brains, with a spatial resolution higher than 2 mm³.

In this paper, a spherical FE model is used to examine the magnitude and extent of the effects of heterogeneity and anisotropy of the brain tissues on the distribution of the electric field induced by TMS. The aim is to assess the expected benefit from building anatomically faithful FE models of individual brains that incorporate conductivity tensor data derived from DT-MRI measurements. A preliminary version of these results was presented at a conference [35].

II. THEORY

The electric field induced by a typical current pulse used in TMS has a frequency spectrum ranging from DC to about 10 kHz. At these low frequencies the quasistatic approximation is valid for most biological tissues [24], [36]. This approximation involves neglecting propagation delays, the shielding effect of the induced currents (skin depth) and any capacitive effects in the conductive medium. The last and weakest assumption, namely that the ratio of displacement to conduction current is much less than unity, appears to be valid even for bone [37].

The total induced electric field can be written in terms of the magnetic vector potential \vec{A} and the electric scalar potential Φ as [22], [38]

$$\vec{E} = -\frac{\partial \vec{A}}{\partial t} - \nabla \Phi \quad (1)$$

In the quasistatic limit, the magnetic vector potential \vec{A} is due solely to the current flowing in the induction coil. The electric scalar potential Φ results from surface charge accumulating at discontinuities in the electrical conductivity.

The conductive medium is assumed to be purely resistive, following a general form of Ohm's law

$$\vec{J} = \underline{\underline{\sigma}} \vec{E} \quad (2)$$

where $\underline{\underline{\sigma}}$ is the conductivity tensor, which can be a function of position. As a consequence, the charge redistribution responsible for Φ follows $\partial \vec{A} / \partial t$ instantaneously. In the quasistatic limit, the divergence of the induced current density is zero and therefore

$$-\nabla \cdot \left(\underline{\underline{\sigma}} \frac{\partial \vec{A}}{\partial t} \right) - \nabla \cdot (\underline{\underline{\sigma}} \nabla \Phi) = 0 \quad (3)$$

If the medium is homogeneous and isotropic then

$$\underline{\underline{\sigma}}(\vec{r}) = \sigma_0 \underline{\underline{I}} \quad (4)$$

where σ_0 is a scalar independent of position \vec{r} and $\underline{\underline{I}}$ is the unit matrix. In this case, the divergence of the electric field is zero and the electric scalar potential Φ obeys Laplace's equation. In an anisotropic medium, the divergence of the electric field is nonzero.

Biological tissues have a relative magnetic permeability very close to unity so the constitutive relation for the magnetic fields is simply

$$\vec{B} = \mu_0 \vec{H} \quad (5)$$

At the tissue/air boundary the current density normal to the surface, $\vec{J} \cdot \vec{n}$, must be zero and so the normal component of $\nabla \Phi$ must satisfy

$$(\underline{\underline{\sigma}} \nabla \Phi) \cdot \vec{n} = - \left(\underline{\underline{\sigma}} \frac{\partial \vec{A}}{\partial t} \right) \cdot \vec{n} \quad (6)$$

where \vec{n} is a unit vector normal to the interface. For a homogeneous isotropic conductor, this boundary condition and Laplace's equation determine Φ .

At the interface between two regions with different conductivities the condition for continuity of current becomes

$$\vec{J}_1 \cdot \vec{n} = \vec{J}_2 \cdot \vec{n} \quad (7)$$

As shown below, this equality is possible because surface charge builds up on the interface, affecting Φ and $\nabla \Phi$ throughout the conductor. In a heterogeneous isotropic medium, the scalar potential obeys Laplace's equation within each homogeneous region. At the tissue/air boundary, the normal component of $\nabla \Phi$ is equal to the normal component of $-\partial \vec{A} / \partial t$, but the solution Φ to Laplace's equation is now subject to additional boundary conditions at the internal interfaces. Thus, the tangential component and, hence, the magnitude, of the electric field at the tissue/air boundary can be affected by the conductor's heterogeneity.

The effect of a boundary between two homogeneous isotropic media with different electrical conductivities on the induced current density and electric field distributions is investigated in more detail using the configuration shown in Fig. 1.¹ It consists of a rectangular inclusion with a high conductivity, σ_1 , in an infinite medium of lower conductivity, σ_2 . Analyzing this geometry is useful for checking the FE results and provides some insight into how the field distributions may be affected by a high conductivity lesion, such as that caused by a cortical stroke, or at

¹This effect is analogous to the one that occurs at the boundary between two media with different electric permittivities or different magnetic permeabilities when placed in an electric or a magnetic field. A solution for a spherical heterogeneity in a uniform field can be obtained analytically [38], [39].

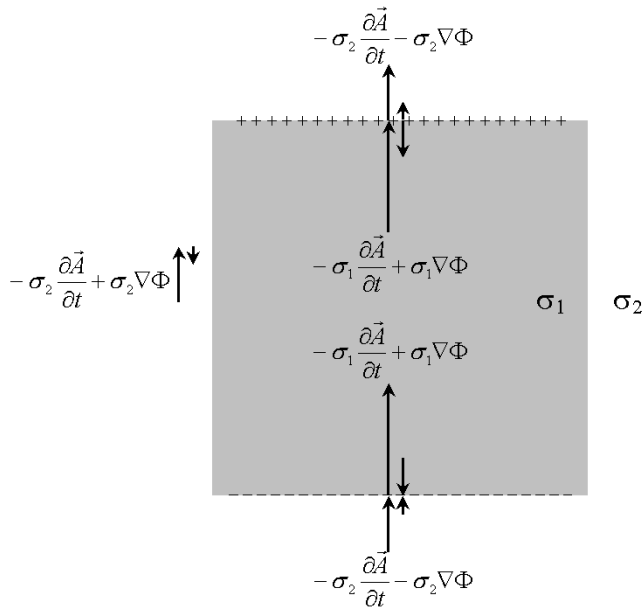


Fig. 1. The effect of an interface between two homogeneous isotropic tissues with different conductivity values ($\sigma_1 > \sigma_2$) on the total induced current density. On each side of an interface the longer arrow represents the primary induced current density $-\sigma_i \partial \vec{A} / \partial t$, which is taken to be perpendicular to the horizontal interfaces. The shorter arrow represents the surface charge contribution $-\sigma_i \nabla \Phi$. The sum of these two contributions is the total normal current density, which must be continuous across the horizontal boundary. This condition determines $\nabla \Phi$.

a cerebrospinal fluid (CSF)—gray matter (GM) interface, such as the one that delimits the motor cortex.

For simplicity, the vector $-\partial \vec{A} / \partial t$ was taken to be uniform throughout the area of interest and perpendicular to the two horizontal interfaces. Due to the difference in the primary induced current density, $-\sigma_i \partial \vec{A} / \partial t$, in the two media, charge builds up at these boundaries. The resulting electric field, $\nabla \Phi$, is also perpendicular to the interfaces and has the same magnitude but opposite direction on the two sides of these interfaces. In Fig. 1, these two contributions to the total normal current density, one due to the magnetic vector potential (longer arrow, $-\sigma_i \partial \vec{A} / \partial t$) and the other due to the surface charge (shorter arrow, $-\sigma_i \nabla \Phi$) are drawn next to each other on each side of an interface. In the steady state, the total normal current density must be continuous across a boundary, which yields the following expression for $\nabla \Phi$ at the boundary, valid in region σ_2 ,

$$\nabla \Phi = \left(\frac{\sigma_1 - \sigma_2}{\sigma_1 + \sigma_2} \right) \frac{\partial \vec{A}}{\partial t}, \quad \sigma_1 > \sigma_2 \quad (8)$$

In region σ_1 , this contribution has the opposite sign.

More generally, if $\partial \vec{A} / \partial t$ is not perpendicular to the interface then, in the low conductivity region

$$\nabla \Phi \cdot \vec{n} = \left(\frac{\sigma_1 - \sigma_2}{\sigma_1 + \sigma_2} \right) \frac{\partial \vec{A}}{\partial t} \cdot \vec{n}, \quad \sigma_1 > \sigma_2 \quad (9)$$

where \vec{n} points in the same direction as the normal component of $\partial \vec{A} / \partial t$. Using the equation above to substitute for $\nabla \Phi$ in the expression for the total normal current density in the low

conductivity region, at the interface with the high conductivity region, gives

$$\vec{J}_2 \cdot \vec{n} = -\sigma_2 \left(\frac{2\sigma_1}{\sigma_1 + \sigma_2} \right) \frac{\partial \vec{A}}{\partial t} \cdot \vec{n} \quad (10)$$

Thus, the normal current density is increased by a factor of $2\sigma_1 / (\sigma_1 + \sigma_2)$ relative to its value in a medium with a uniform low conductivity. The normal component of the electric field is also increased by the same factor. These components will tend to their unperturbed values as the distance from the interface increases.

Within the high conductivity region the normal current density is

$$\vec{J}_1 \cdot \vec{n} = -\sigma_1 \left(\frac{2\sigma_2}{\sigma_1 + \sigma_2} \right) \frac{\partial \vec{A}}{\partial t} \cdot \vec{n} = \vec{J}_2 \cdot \vec{n} \quad (11)$$

i.e., it is decreased by a factor of $2\sigma_2 / (\sigma_1 + \sigma_2)$ relative to its values in a uniform high conductivity medium but still increased by a factor of $2\sigma_1 / (\sigma_1 + \sigma_2)$ relative to its value in a medium with a uniform low conductivity. The normal component of the electric field is decreased by a factor of $2\sigma_2 / (\sigma_1 + \sigma_2)$.

The magnitude of the current density in the high conductivity region is larger than in the low conductivity region since its normal component is continuous at the interface. The opposite is true for the electric field given that its tangential component is continuous at interfaces. Thus, the directions of \vec{J} and \vec{E} are neither continuous across the interface nor parallel to $\partial \vec{A} / \partial t$ in its vicinity. Additionally, the effect of heterogeneity on the electric field and current density distributions is directional: in isotropic media, it is greatest when $\partial \vec{A} / \partial t$ is normal to the interface and absent when it is parallel to the interface.

In the low conductivity region adjacent to the neutral interfaces [Fig. 1 (left)] the component of both fields parallel to that interface is also decreased by a factor of $2\sigma_2 / (\sigma_1 + \sigma_2)$, assuming that $\nabla \Phi$ is uniform in region σ_1 ,² and neglecting end effects. If $\partial \vec{A} / \partial t$ is not parallel to one set of interfaces then both the normal and the tangential components of \vec{J} and \vec{E} will be affected everywhere in and around the rectangle.

For $\sigma_1 = 1.79 \text{ S} \cdot \text{m}^{-1}$ (CSF [40]) and $\sigma_2 = 0.4 \text{ S} \cdot \text{m}^{-1}$ (GM, [41]–[45]) the normal component of the vector fields in the low conductivity region is increased by a factor of 1.63 whereas in the high conductivity region it is decreased by a factor of 0.37. In the low conductivity region next to the neutral interfaces, the tangential component of both fields is also decreased by a factor of 0.37, approximately.

In the above calculations, only the effect of charge accumulating on the interface of interest on the local current density, $-\sigma_i \nabla \Phi$, was taken into account when enforcing current continuity [(7)–(11)]. Charge will also build up on other interfaces adding another contribution to the total current density at the interface of interest, $-\sigma_i \nabla \Phi'$, that may be significant. This second contribution depends on the relative position and orientation of the other interfaces and will, in general, have to be accounted for numerically, using the FE method for example.

²Uniformity is achieved only in a spherical or ellipsoidal heterogeneity [38]. This approximation improves as the distance between the charged surfaces decreases relative to the other dimensions.

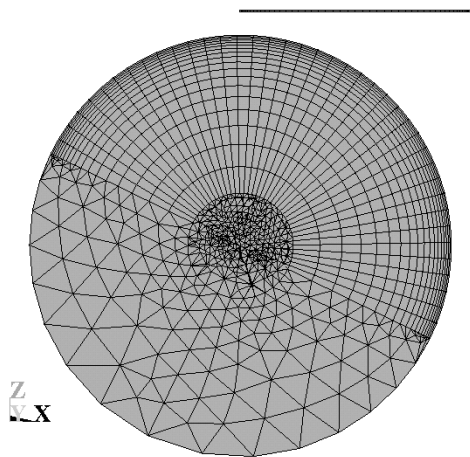


Fig. 2. Central section through the 3-D mesh used in the FE calculations, passing through the centers of the sphere and of the circular coil. The center of the sphere is located at the origin of the reference frame, whose y axis points into the paper (bottom left). The elements representing the air and the infinite boundary are omitted. Radius of the sphere: 9.2 cm; coil diameter: 10 cm; sphere-coil separation: 1.0 cm; rate of change of current: $100 \text{ A} \cdot \mu\text{s}^{-1}$.

One effect of anisotropy is that \vec{J} will in general not be parallel to \vec{E} , even in homogeneous media, since the tensor $\underline{\sigma}$ scales and rotates \vec{E} . As a result, the magnitude of the electric field induced on the outer boundary of a homogeneous anisotropic conductor is not the same as if the conductor were isotropic. At this boundary the normal component of the current density must still be zero but since

$$\vec{E} = \underline{\sigma}^{-1} \vec{J} \quad (12)$$

the normal component of the electric field is not necessarily zero [46].

III. METHODS

Calculations of the electric field and current distributions induced in a spherical conductor were performed using the electromagnetic module of the finite-element package ANSYS, version 5.6 (ANSYS Inc., <http://www.ansys.com>). The FE method was chosen because of its ability to model heterogeneous and anisotropic conductors of arbitrary shape accurately.

The element type chosen for these calculations (Solid 97) uses a magnetic potential formulation incorporating the Coulomb gauge to solve (2), (3), (5), and Ampère's law for \vec{A} and $\nabla\Phi$ subject to the appropriate boundary conditions [47]. In fact, skin depth is not neglected but its effect on the calculations presented here is not significant. The elements are linear and can be either hexahedral or tetrahedral. The frontal solver was used. The fundamental output of the program is a list of the three cartesian components of the total current density calculated at each element's centroid. The components of the electric field are derived by applying (12) in the element's orthotropic frame of reference.

The solid model consists of a conducting sphere 9.2 cm in diameter [23], a coil 10 cm in diameter with a cross section of $0.1 \text{ cm} \times 0.1 \text{ cm}$ and a surrounding concentric sphere of air. In this model, the brain surface would lie 1.2 cm below the surface of the conducting sphere. The mid-plane of the 10-turn coil was placed 1.0 cm above the vertex of this sphere (cf. Fig. 2). The

linear dimension of the coil's cross section is small compared with the distance separating it from the head so that the FE results may be compared with theoretical values for a line coil.

Hexahedral elements were used to mesh the head near the coil where the magnetic vector potential varies rapidly with distance. In this region, it quickly became clear that even a large number of linear tetrahedral elements could not achieve sufficient accuracy. The mesh was refined until an acceptable accuracy was attained in a reasonable CPU time.

The coil was driven by an independent current source that ramped the current through all its nodes at a constant rate of $100 \text{ A} \cdot \mu\text{s}^{-1}$. Given the cylindrical symmetry of the current carrying conductor, the nontangential components of \vec{A} were set to zero. A third concentric sphere of special open boundary elements (Infin111) was used to apply the only necessary explicit boundary condition, i.e. \vec{A} tends to zero as the distance from the coil increases.

The accuracy of the FE calculations was ascertained by comparison with the results obtained by numerical evaluation of Eaton's analytical formulas for the electric field induced in a homogeneous sphere by an arbitrarily shaped coil [48]. These formulas neglect propagation effects and skin depth and were first simplified so as to neglect capacitive effects as well. Further simplifications reflecting the symmetry of the round coil were carried out before numerical evaluation using Mathematica, version 4.0 (Wolfram Research, Inc., <http://www.wolfram.com>). The electric field was evaluated at the centroid of the elements used in the FE calculation. A twentieth order approximation was used in the summations.

In the special case where the axis of the round coil passes through the center of the homogeneous spherical conductor, no charge builds up on the sphere's surface. The electric field distribution is determined solely by the coil geometry via Biot-Savart's law. The expression for the magnetic vector potential generated by a round coil is given in Smythe [49] and was also evaluated using Mathematica.

The results from four different calculations are reported in this paper. The first two are validations of the FE calculations in homogeneous isotropic media and the other two explore the effect of heterogeneity and anisotropy on the electric field and current density distributions. The results are shown as smoothed contour plots of the magnitude of the vector fields but the numbers reported represent actual values calculated at the element centroid. In some plots, the sphere is cut at a plane to expose the contours in that plane. Only the results from the top hemisphere are plotted in figures.

In the first calculation, the coil was centered over a homogeneous isotropic sphere. The conductivity was set to that of GM, $0.4 \text{ S} \cdot \text{m}^{-1}$. The electric field and current density distributions were calculated using the formula in Smythe, Eaton's formula, and the FE method. One of the purposes of this calculation was to validate our implementation of Eaton's formula before using it in the second calculation. In the second calculation, the coil was displaced by one coil radius in a direction perpendicular to the coil's axis. This is approximately the coil position used during stimulation of the motor cortex. In this situation, only Eaton's formula and the FE method can give correct results since $\nabla\Phi$ is no longer zero. The direction of the

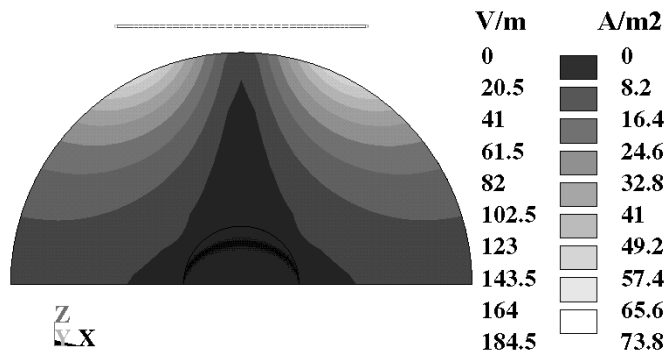


Fig. 3. Central section through the top hemisphere. Contour plot of the FE solution for the magnitude of the electric field ($V \cdot m^{-1}$) or current density ($A \cdot m^{-2}$) induced by a current flowing in a round coil centered over a sphere of conductivity $0.4 S \cdot m^{-1}$. The direction of the current density or electric field vector is perpendicular to the plane of the figure.

coil's displacement was taken as the x axis and the plane of the coil as the x - y plane (cf. Fig. 2).

In the third calculation, a high conductivity inclusion was embedded in the sphere, near the surface below the vertex. The conductivity of the inclusion was taken to be that of CSF, $1.79 S \cdot m^{-1}$. In the fourth calculation, the conductivity was homogeneous but anisotropic. The direction of highest conductivity pointed 30° away from the x axis and from the x - y plane (-30° rotation about the y axis). Along this direction the conductivity was set to $0.72 S \cdot m^{-1}$ whereas along the other two it was set to $0.24 S \cdot m^{-1}$. Its average value remained equal to that used for the homogeneous sphere. The offset coil position was also used in these last two calculations.

All programs were run on a SUN Ultra 60 workstation with dual 250-MHz processors and 1 GB of RAM.

IV. RESULTS

The central cross section of the three-dimensional (3-D) mesh used in the FE calculations is shown in Fig. 2. It consists of a total of 66 644 linear elements, 21 600 of which are hexahedral and are concentrated in the top hemisphere, inner core excluded. These are the elements over which the accuracy of the calculation was tested since stimulation will not take place in the lower hemisphere. About 12 h of CPU time were required to run each calculation.

The magnitude of the electric field induced by the coil centered on the homogeneous sphere is shown in Fig. 3. The current density distribution follows the same pattern and its values differ only by a scaling factor since the medium is isotropic. The maximum values are $184 V \cdot m^{-1}$ and $73.4 A \cdot m^{-2}$, respectively, and occur at the surface of the sphere, approximately under the winding. As shown in Fig. 4, the largest difference between these FE results and those calculated using Eaton's formulas amounts to -6.7% of the reference (i.e. Eaton's) value and is also located on the surface near the maximum values. Slightly deeper, where the GM is located, the absolute value of this error falls below 5%. The z component and the radial component, which should be strictly zero, represent at most 0.2% of the maximum magnitude. The values calculated using Eaton's

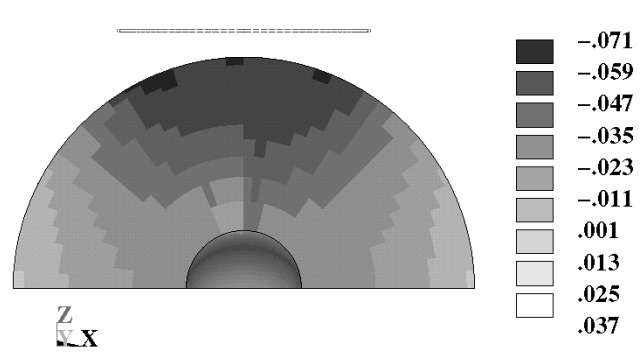


Fig. 4. Contour plot of the difference between the electric field or current density magnitude calculated using the FE method (Fig. 3) and the corresponding theoretical values calculated using Eaton's analytical formulas, expressed as a fraction of the theoretical value.

formulas and Smythe's formula differ by less than 0.3% when values greater than 20% of the maximum value are considered. This small difference is attributed to the truncation of the infinite series in Eaton's formulas and the finite precision with which the integrals in Smythe's formulas are evaluated numerically.

The results from the second FE calculation are shown in Fig. 5. The coil is now offset and the induced surface charge alters the electric field and current density distributions. The maximum magnitude of both vector fields occurs near the vertex of the sphere, with values of $209 V \cdot m^{-1}$ and $83.4 A \cdot m^{-2}$, respectively. The difference between the FE and the reference values reaches -6% near the vertex and its absolute value is down to about 5% in the stimulation region, as shown in Fig. 6. The largest difference, -8.3% , occurs in a low field region. The radial component represents less than 0.2% of the maximum magnitude. The magnitude of the reference electric field 15 mm below the vertex is $107 V \cdot m^{-1}$. For an 8-turn coil this figure scales down to $86 V \cdot m^{-1}$, which is in reasonable agreement with the equivalent figure of $89 V \cdot m^{-1}$ given in Roth [23].

The effect of a high conductivity inclusion on the electric field and on the current density distribution is shown in Fig. 7. The inclusion is located between 0.9 and 2.2 cm below the vertex and occupies $4.5 cm^3$ (cf. Figs. 8 and 9). Within each region the media are isotropic and so the electric field and current density vectors are still parallel, albeit with different proportionality constants for each region. In the case of a high conductivity inclusion, the current density maximum is localized in depth even though the electric field maximum still occurs at the surface. Fig. 8 shows the change in the vector fields in the low conductivity region caused by the presence of the high conductivity inclusion. It is a plot of the difference in the magnitude of the vector fields between the heterogeneous and the homogeneous spheres (Fig. 7 and Fig. 5), in which the values from the high conductivity elements have been excluded. The field magnitude is increased along the direction of current flow and is decreased perpendicular to it. At the two interfaces that are almost perpendicular to the current flow the field magnitude is increased by a factor of 1.43. This boost still maintains approximately one third of its maximum value 8 mm away from the interface. A reduction in the thickness of the inclusion along the y axis, from

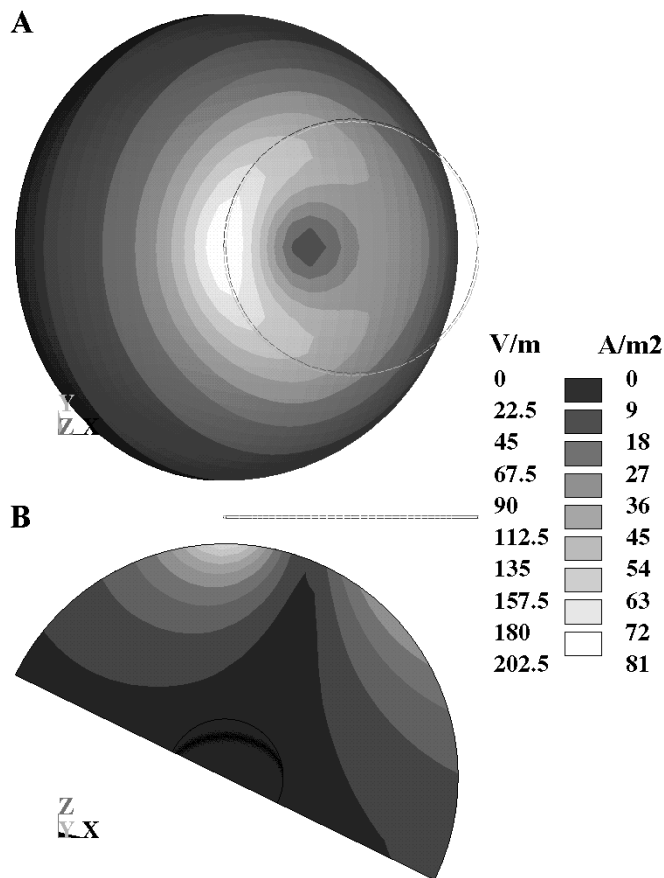


Fig. 5. Contour plots of the FE solution for the magnitude of the electric field ($\text{V} \cdot \text{m}^{-1}$) or current density ($\text{A} \cdot \text{m}^{-2}$) induced by a current flowing in a round coil placed asymmetrically over a sphere of conductivity $0.4 \text{ S} \cdot \text{m}^{-1}$. The scales apply to both plots. (A) View from above the coil; (B) central section.

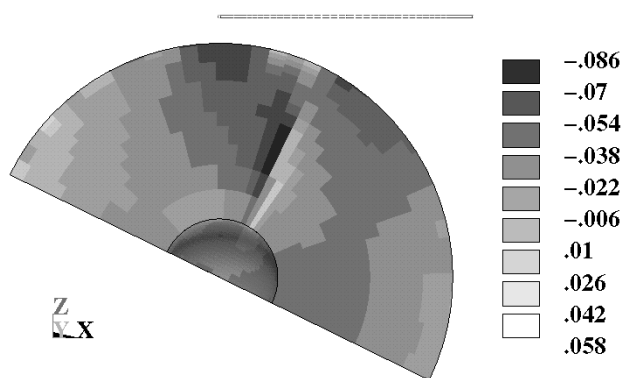


Fig. 6. Difference between the FE values plotted in Fig. 5 and the corresponding theoretical values, expressed as a fraction of the theoretical value.

2.0 cm to 0.6 cm, did not show a significant effect on the penetration of the electric field increase into the low conductivity region.

The radial components of the electric field and current density at the boundary, which should be strictly zero, are still small: 1.2% and 0.7% of the respective maximum magnitudes. However, in the vicinity of the upper and lower edges of the inclusion that are parallel to the x axis (i.e. approximately perpen-

dicular to the current flow) this radial component is significant, as shown in Fig. 9. Above the upper edges of the inclusion the radial component of the electric field reaches 22% of the maximum or 38% of the local magnitude. Inside the inclusion, near the lower edges the radial current density reaches 18% of the maximum magnitude or 36% of the local magnitude.

In Fig. 8, the inclusion was positioned below the vertex in order to reproduce as closely as possible the geometry shown in Fig. 1. In another calculation (not shown), we positioned the inclusion approximately where the motor cortex would be located in this spherical model and found a similar spatial pattern of field intensification and reduction, but skewed with respect to the orientation of the interfaces because $\partial \vec{A} / \partial t$ was not perpendicular to any of the boundaries.

The effect of anisotropy on the electric field and current density distributions is shown in Fig. 10. Again, the maximum magnitude of both vector fields occurs near the vertex of the sphere, with values of $46.7 \text{ A} \cdot \text{m}^{-2}$ and $194.2 \text{ V} \cdot \text{m}^{-1}$, respectively. However, the two distributions are clearly different from each other and from that illustrated in Fig. 5. The highest current density contour extends further back along the circular ridge of high values that encloses the local superficial minimum [Fig. 10(C)]. It represents lower values than those shown in Fig. 5 due to the lower conductivity along the y axis ($\sigma = 0.24 \text{ S} \cdot \text{m}^{-1}$). In absolute terms, the electric field is increased at the back of the ridge, 180° from the maximum, reflecting the altered charge distribution caused by the higher conductivity along the x axis ($\sigma = 0.72 \text{ S} \cdot \text{m}^{-1}$) relative to the other directions.

The radial components of the vector fields have two extrema of opposite sign, symmetrically placed about the central xz -plane, at approximately $y = \pm 3 \text{ cm}$. The radial component of the electric field is largest on the surface of the sphere, as shown in Fig. 11, and reaches 28% of the maximum electric field magnitude. Approximately on the same plane, the radial component of the current density has a minimum located in depth that represents 4.9% of the maximum magnitude. At the surface, its value is down to 1.2% of its maximum magnitude.

V. DISCUSSION

The results obtained to validate the FE model of a homogeneous isotropic sphere show that the magnitude of the vector fields can be calculated with an error of about 5% in the region of interest, even in the presence of a large surface charge contribution. The calculations can be done with sufficient accuracy in a reasonable computation time provided the mesh is carefully designed. The magnitude of the current density appears to be systematically underestimated in the vicinity of the coil and slightly overestimated over a larger volume further from the coil.

These estimates for the accuracy of the FE solution for the homogeneous isotropic sphere cannot be automatically extended to the last two calculations mainly because heterogeneity and anisotropy introduce new field patterns for which the mesh was not optimized. Heterogeneity also introduces new internal interfaces whose boundary conditions are handled naturally by the FE method. The errors associated with the last two calculations are probably not much larger than those associated with the first

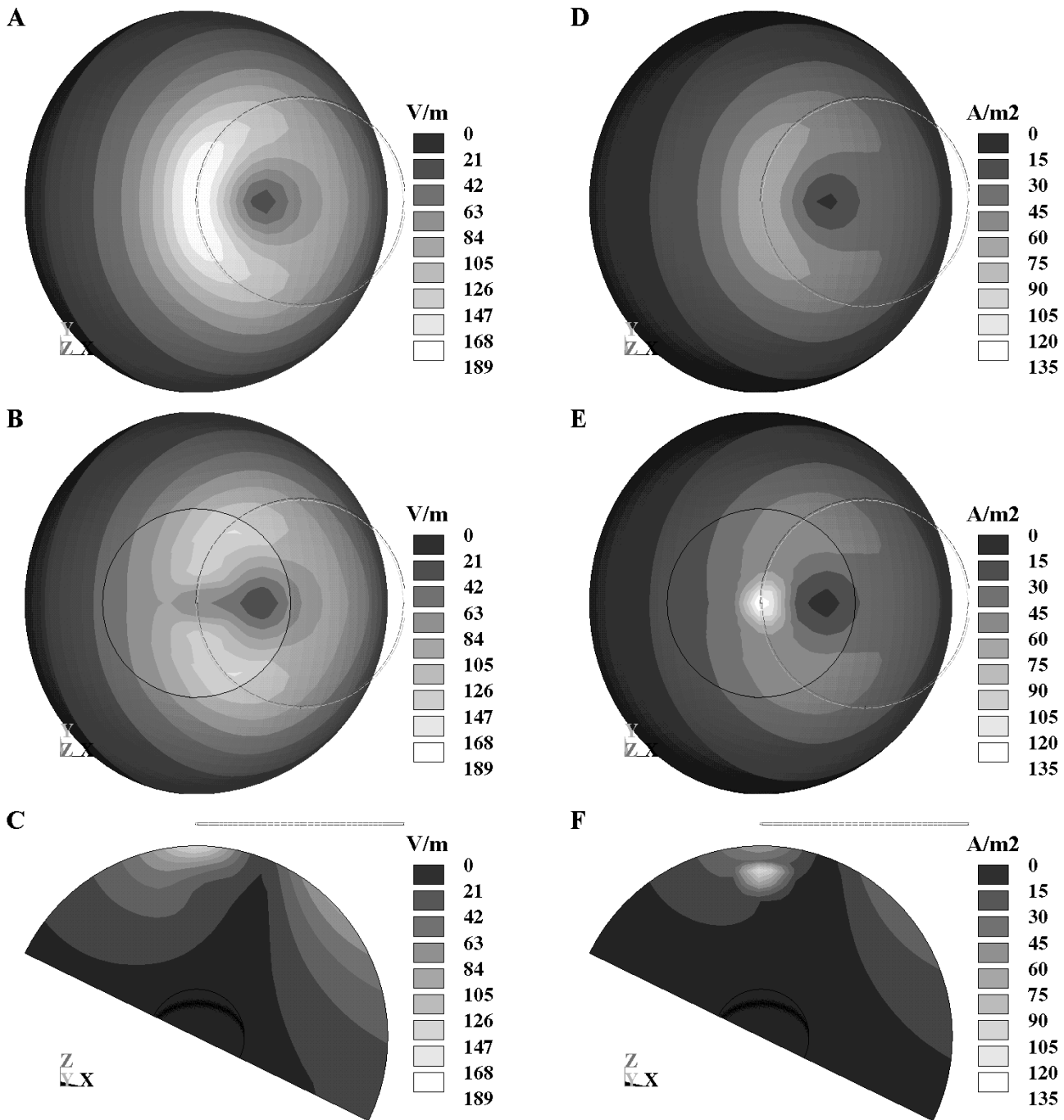


Fig. 7. Magnitude of the electric field, in $V \cdot m^{-1}$ (column on the left), and current density, in $A \cdot m^{-2}$ (column on the right), induced by a current flowing in a round coil placed asymmetrically over a heterogeneous sphere. The effect of the inclusion with a conductivity of $1.79 S \cdot m^{-1}$ is visible on all views. (A), (D) View from above the coil; (B), (E) $x-y$ section through the inclusion; (C), (F) $x-z$ section through the inclusion.

two and are very likely to be smaller than the uncertainty with which the conductivity tensor can be determined *in vivo*.

In the FE model, the changes introduced by a high conductivity inclusion in a low conductivity medium follow the predicted pattern. The electric field within the inclusion is decreased due to the shielding effect of the surface charge that builds up on the interface, Fig. 7(B). This effect is more than offset by the high conductivity value in the inclusion, which makes the current density there higher than outside, Fig. 7(E).

Outside the inclusion both fields are increased along the direction of current flow and decreased in the plane perpendicular to it, Fig. 8. The FE calculations show that the magnitude of the fields in the vicinity of the high conductivity inclusion is increased by a factor of 1.43, which is in reasonable agreement with the value predicted in Section II: 1.63 at the interface. The difference is probably due to two factors: 1) the magnitude of the fields is calculated at the centroid of the elements, 2–3 mm away from the interface, and the magnitude of the fields varies

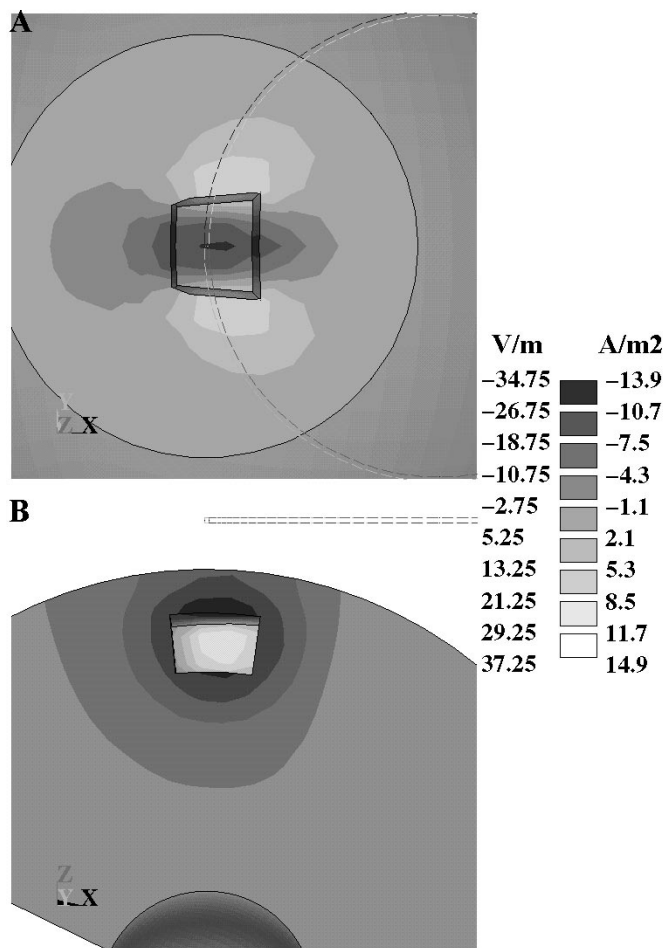


Fig. 8. Difference between the electric field or current density magnitude plotted in Fig. 7 and the corresponding values in a homogeneous sphere (Fig. 5) in the low conductivity volume. (A) The $x-y$ section at the level of the inclusion. (B) The $x-z$ section at the level of the inclusion. The values plotted inside the “boxes” pertain to the low conductivity region, now visible at the bottom of the “pit” left by the removal of the high conductivity elements.

rapidly with position and 2) changes in the charge distribution on other nearby boundaries alter the total electric field induced at the interface under consideration.

In the anisotropic sphere model, the conductivity along the direction of maximum electric field and current density, the y axis, was reduced from $0.4 \text{ S} \cdot \text{m}^{-1}$ to $0.24 \text{ S} \cdot \text{m}^{-1}$. In the absence of an outer boundary, the maximum magnitude of the electric field would be unaltered and that of the current density would be reduced by a factor of 0.6. The calculated ratios are 7% lower, 0.93 and 0.56, respectively. A small difference was expected due to the new charge distribution required to satisfy the new boundary condition $(\underline{\sigma}\underline{E}) \cdot \underline{n} = 0$ and the curved shape of the boundary.

Significant radial components of the electric field and current density were found in both the heterogeneous and the anisotropic FE sphere, but not in the homogeneous isotropic models. In the heterogeneous sphere, both radial components tend to zero near the outer boundary, as expected. It is only in a very limited volume, close to the nonradial edges of the planes perpendicular to current flow, that the radial components have significant values. In the case of the anisotropic sphere, only

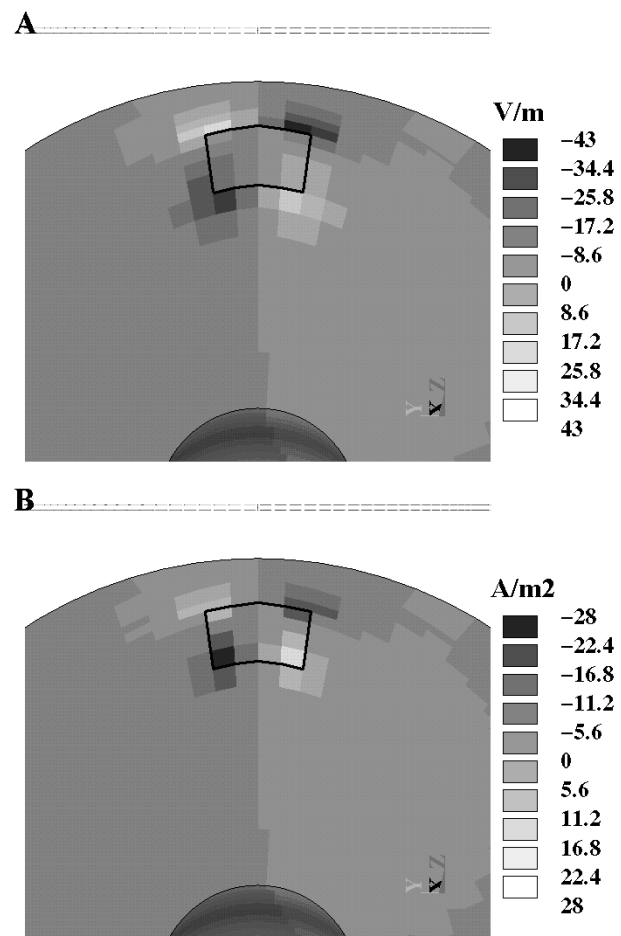


Fig. 9. Plots of the radial component of the vector fields in a heterogeneous sphere. The border of the inclusion is outlined with a black line. The contours inside and outside the inclusion are shown. (A) Radial electric field, $y-z$ section at $x = 0$. (B) Radial current density, $y-z$ section at $x = 0$. Note the reduction in the intensity scale relative to Fig. 7.

the radial current density tends to zero near the boundary, as required, whereas the radial component of the electric field is largest there. The nonzero values of the radial current density at the boundary reflect the finite accuracy of this calculation.

The calculation of the electric field distribution induced by magnetic stimulation in a homogeneous isotropic conductor is essentially a geometry problem, where the coil geometry determines $\partial\vec{A}/\partial t$ and the boundary geometry determines $\nabla\Phi$. However, heterogeneity and anisotropy make the field distribution also dependent on the distribution of material properties and on the geometry of the resulting internal boundaries. It was shown here that these characteristics can introduce significant changes in the electric field distribution for physiological values of the conductivity properties. In principle, the results from these calculations can be verified experimentally using suitable phantoms.

The brain is a heterogeneous, anisotropic conductive medium where the effects illustrated above are bound to occur. CSF is highly conducting and isotropic. The average or bulk conductivity of GM is approximately 4 times less than that of CSF. White matter (WM) has an average conductivity of about $0.2 \text{ S} \cdot \text{m}^{-1}$ [41], [43], some 2 times lower than that of GM. WM

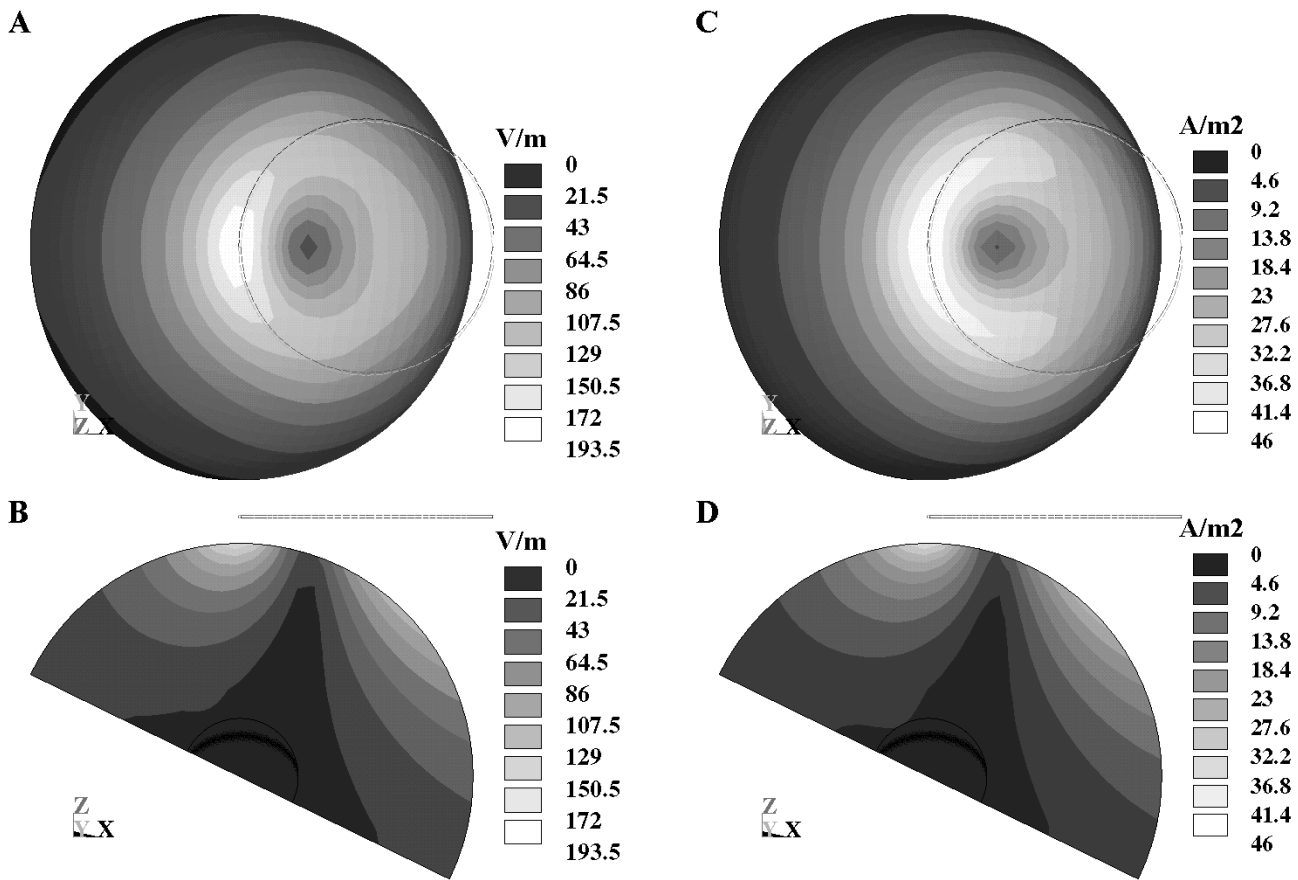


Fig. 10. Magnitude of the electric field ($V \cdot m^{-1}$) and the current density ($A \cdot m^{-2}$) induced by a current flowing in a round coil placed asymmetrically over an anisotropic sphere. The eigenvalues of the conductivity tensor were set to $\sigma_{XX} = 0.72 S \cdot m^{-1}$, $\sigma_{YY} = \sigma_{ZZ} = 0.24 S \cdot m^{-1}$, and the tensor was rotated by -30° about the y axis (X toward Z). (A), (C) View from above the coil; (B), (D) central section.

is anisotropic, with a conductivity along the fiber direction that can be as much as nine times higher than in the perpendicular direction; its longitudinal conductivity can be as high as about $1 S \cdot m^{-1}$ and its transverse conductivity as low as about $0.1 S \cdot m^{-1}$ [50], [51].

Given the diverse conductivity values that can be found in the brain, significant increases and decreases in the electric field can be expected at boundaries between different tissues. Fig. 12 illustrates schematically the sort of effects that may take place at the GM-CSF and GM-WM interfaces, as explained below. Since the induced electric field is predominantly tangential to the scalp, these effects occur in the walls of the sulci and not at the crown of the gyri.

It was shown in the theory section that the GM-CSF interface can potentially increase the electric field in the GM region by a factor of about 1.6 when the induced current is flowing perpendicularly to that interface. This is a significant effect considering that magnetic stimulation is often performed at about 1.1 or 1.2 times the threshold intensity.

Such a situation arises during magnetic stimulation of the motor cortex, which lies anterior to a CSF filled sulcus, the central sulcus (cf. right inset, Fig. 12). For lowest threshold stimulation the coil is oriented so as to make the induced current flow approximately perpendicular to the plane of the sulcus, in the posterior-anterior direction [52]. This may simply correspond to optimizing the electric field boost in GM and would pref-

erentially affect axons that are perpendicular to the GM-CSF boundary. The same increase would occur at the GM-CSF interface of the somatosensory cortex, which lies posterior to the central sulcus, or in any cortical tissue adjacent to a sulcus that lies approximately perpendicular to the induced current flow. Even though the increase in the electric field induced in GM in contact with CSF takes place on both sides of a sulcus, the induced current direction will be optimal for stimulation (from CSF into GM) at only one of those interfaces.

In the motor cortex, the shortest latency responses can be obtained by placing the stimulation coil in such a way that the induced current flows approximately parallel to the central sulcus [53], i.e. perpendicular to the paper in Fig. 12. These responses have a higher threshold that could be due in part to the absence of the boost effect, in addition to eventual differences in cell excitability.

The situation at a WM-GM interface is less clear. In the sulci, it appears that the WM fibers run parallel to the WM-GM interface and then turn sharply through about 90° as they enter the GM. Taking the WM conductivity normal to the boundary to be its transverse conductivity, say $0.1 S \cdot m^{-1}$ and that of GM to be $0.4 S \cdot m^{-1}$ would result in an decrease in the normal component of electric field in the GM by a factor of 0.4 and an increase in the WM by a factor of 1.6 (cf. left inset, Fig. 12). In this case, there would be two faces to GM: the interface with CSF where the normal component of the electric field would be

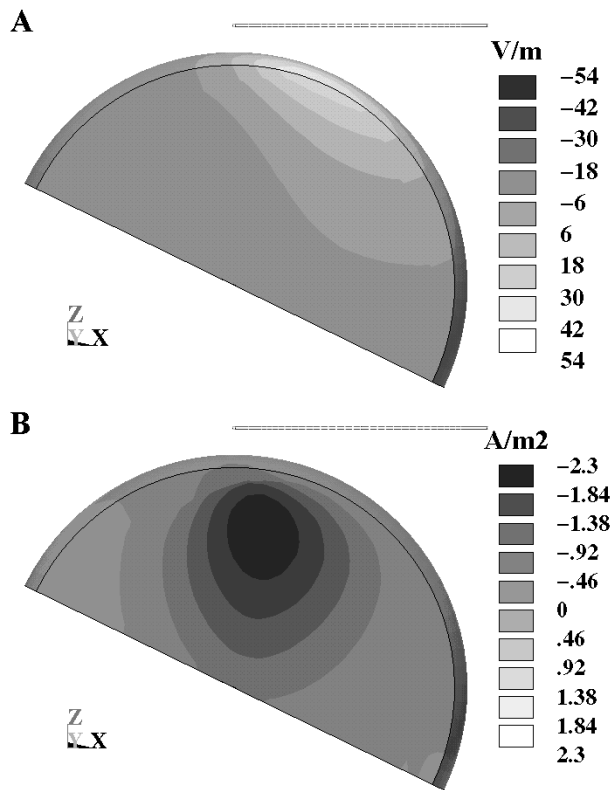


Fig. 11. The radial component of the vector fields in an anisotropic sphere. The inner semi-circular line represents the edge created by cutting the sphere at the plane $y = -3.0$ cm. (A) Radial electric field, whose maximum value occurs at the surface. (B) Radial current density, whose value is maximum in depth and approaches zero at the surface. Note the reduction in scale relative to Fig. 10.

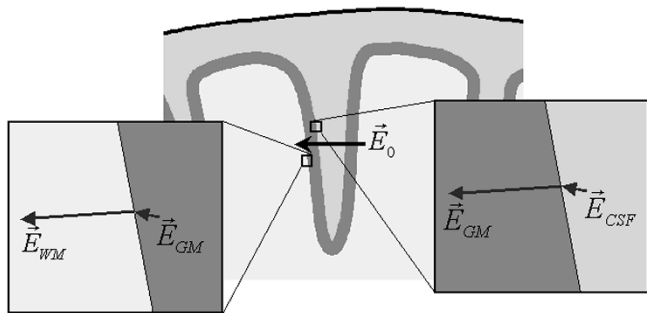


Fig. 12. Sketch of the effect of conductivity boundaries on the total induced electric field, drawn on a perpendicular section through an idealized sulcus. The central horizontal vector indicates the direction and magnitude of the induced electric field \vec{E}_0 in a homogeneous, isotropic conductor. Right inset: GM-CSF interface, with $\sigma_{GM} = 0.4 \text{ S} \cdot \text{m}^{-1}$ and $\sigma_{CSF} = 1.79 \text{ S} \cdot \text{m}^{-1}$. Left inset: GM-WM interface, with $\sigma_{WM} = 0.1 \text{ S} \cdot \text{m}^{-1}$. The vectors on either side of an interface represent the total induced electric field, taking into account the effect of charge accumulation at that boundary (10), (11). Their lengths are scaled appropriately relative to that of \vec{E}_0 and their directions deviate from horizontal because \vec{E}_0 is not exactly perpendicular to the interface (approximately 10° off in this illustration).

enhanced, and the interface with WM where the electric field would be reduced. Nevertheless, stimulation at the GM-WM

interface should not be excluded because the sharp turns of the axons could provide sufficiently low threshold points.

The anisotropy of the WM that underlies the superficial GM could, in principle, introduce a radial component of the electric field in the GM that may lead to stimulation of neurons in the crown of the gyri. However, this component can only represent a fraction of the total magnitude and is, therefore, likely to be effective only for high stimulus intensities. In regions where anisotropic, high conductivity bundles of WM fibers turn sharply, such as the U-fibers which connect the motor and somatosensory cortices, the electric field can also be enhanced along the outer edges of the bend.

The above considerations indicate that the distribution of the electric field induced in the brain is likely to exhibit a myriad of “hot spots” that can influence the location and the extent of the territory effectively stimulated. The nature of these “hot spots” depends on the geometry of the local interfaces and on the conductive properties of the tissues involved. This implies that there is no simple, smoothly varying spatial relationship between the position of the coil on the scalp and the site(s) where stimulation may occur.

A more detailed assessment of the effects of tissue heterogeneity and anisotropy can be obtained by using a realistic FE model of the head incorporating high-resolution conductivity data derived from DT-MRI measurements. Such models should also be useful in predicting the electric field distribution induced in the brain of patients who have suffered cortical strokes. The calculations presented in this paper indicate that the location and extent of the stimulated region may be considerably affected by the proximity of a high conductivity lesion.

FE models integrating DT-MRI derived conductivity data may also be useful in determining the site of excitation during magnetic stimulation of the peripheral nervous system. One possible application would be the stimulation of spinal nerve roots where the geometry of the surrounding bone structure plays a major role in shaping the distribution of the electric field and that of its gradient [25].

Given the electric field distribution it is possible to calculate the distribution of the electric field gradient as well as their components along specific directions, such as the direction of large fiber tracts or the normal to the GM surfaces. This kind of knowledge about the spatial distribution of the current density, the electric field and the electric field gradient is potentially useful for designing TMS experiments that aim to determine the effective activation function for stimulation of brain tissues.

VI. CONCLUSION

In this paper, the FE method was used to calculate three-dimensional distributions of electric fields and current densities induced in models of brain tissue during magnetic stimulation. The results show that the level of tissue heterogeneity and anisotropy present in the brain can alter significantly the induced electric field distribution in GM. FE conductivity models of the head based on DT-MRI data are expected to provide a better understanding of the location of possible stimulation sites in the brain.

REFERENCES

- [1] R. G. Bickford and B. D. Fremming, "Neuronal stimulation by pulsed magnetic fields in animals and man," in *Tech. Dig. 6th Int. Conf. Med. Electron. Biol. Eng.*, 1965.
- [2] M. J. R. Polson, A. T. Barker, and I. L. Freeston, "Stimulation of nerve trunks with time-varying magnetic fields," *Med. Biol. Eng. Comput.*, vol. 20, pp. 243–244, 1982.
- [3] A. T. Barker, R. Jalinous, and I. L. Freeston, "Non-invasive magnetic stimulation of human motor cortex," *Lancet*, vol. ii, pp. 1106–1107, 1985.
- [4] M. Hallett, "Transcranial magnetic stimulation and the human brain," *Nature*, vol. 406, pp. 147–150, 2000.
- [5] R. Q. Cracco, J. B. Cracco, P. J. Maccabee, and V. E. Amassian, "Cerebral function revealed by transcranial magnetic stimulation," *J. Neurosci. Meth.*, vol. 86, pp. 209–219, 1999.
- [6] M. Jahanshahi and J. Rothwell, "Transcranial magnetic stimulation studies of cognition: An emerging field," *Exp. Brain Res.*, vol. 131, pp. 1–9, 2000.
- [7] V. Walsh and A. Cowey, "Transcranial magnetic stimulation and cognitive neuroscience," *Nature Rev. Neurosci.*, vol. 1, pp. 73–79, 2000.
- [8] M. S. George, Z. Nahas, M. Molloy, A. M. Speer, N. C. Oliver, X. Li, G. W. Arana, S. C. Risch, and J. C. Ballenger, "A controlled trial of daily left prefrontal cortex TMS for treating depression," *Biol. Psych.*, vol. 48, pp. 962–970, 2000.
- [9] V. E. Amassian, L. Eberle, P. J. Maccabee, and R. Q. Cracco, "Modeling magnetic coil excitation of human cerebral cortex with a peripheral nerve immersed in a brain-shaped volume conductor: The significance of fiber bending in excitation," *Electroencephalogr. Clin. Neurophysiol.*, vol. 85, pp. 291–301, 1992.
- [10] P. J. Maccabee, V. E. Amassian, L. P. Eberle, and R. Q. Cracco, "Magnetic coil stimulation of straight and bent amphibian and mammalian peripheral nerve *in vitro*: Locus of excitation," *J. Physiol. (Lond.)*, vol. 460, pp. 201–219, 1993.
- [11] S. S. Nagarajan, D. M. Durand, and K. Hsuing-Hsu, "Mapping location of excitation during magnetic stimulation: Effects of coil position," *Ann. Biomed. Eng.*, vol. 25, pp. 112–125, 1997.
- [12] S. S. Nagarajan, D. M. Durand, and E. N. Warman, "Effects of induced electric fields on finite neuronal structures: A simulation study," *IEEE Trans. Biomed. Eng.*, vol. 40, pp. 1175–1188, Nov. 1993.
- [13] B. J. Roth and P. J. Basser, "A model of the stimulation of a nerve fiber by electromagnetic induction," *IEEE Trans. Biomed. Eng.*, vol. 37, pp. 588–597, 1990.
- [14] —, "Erratum to 'A model of the stimulation of a nerve fiber by electromagnetic induction'," *IEEE Trans. Biomed. Eng.*, vol. 39, p. 1211, Nov. 1992.
- [15] P. J. Basser and B. J. Roth, "Stimulation of a myelinated nerve axon by electromagnetic induction," *Med. Biol. Eng. Comput.*, vol. 29, pp. 261–268, 1991.
- [16] J. Nilsson, M. Panizza, B. J. Roth, P. J. Basser, L. G. Cohen, G. Caruso, and M. Hallett, "Determining the site of stimulation during magnetic stimulation of a peripheral nerve," *Electroencephalogr. Clin. Neurophysiol.*, vol. 85, pp. 253–264, 1992.
- [17] V. E. Amassian, P. J. Maccabee, R. Q. Cracco, J. B. Cracco, M. Somasundaram, J. C. Rothwell, L. Eberle, K. Henry, and A. P. Rudell, "The polarity of the induced electric field influences magnetic coil inhibition of human visual cortex: Implications for the site of excitation," *Electroencephalogr. Clin. Neurophysiol.*, vol. 93, pp. 21–26, 1994.
- [18] T. Krings, B. R. Buchbinder, W. E. Butler, K. H. Chiappa, H. J. Jiang, G. R. Cosgrove, and B. R. Rosen, "Functional magnetic resonance imaging and transcranial magnetic stimulation: Complementary approaches in the evaluation of cortical motor function," *Neurology*, vol. 48, pp. 1406–1416, 1997.
- [19] B. Boroojerdi, H. Foltys, T. Krings, U. Spetzger, A. Thron, and R. Topper, "Localization of the motor hand area using transcranial magnetic stimulation and functional magnetic resonance imaging," *Clin. Neurophysiol.*, vol. 110, pp. 699–704, 1999.
- [20] E. M. Wassermann, B. Wang, T. A. Zeffiro, N. Sadato, A. Pascual-Leone, C. Toro, and M. Hallett, "Locating the motor cortex on the MRI with transcranial magnetic stimulation and PET," *NeuroImage*, vol. 3, pp. 1–9, 1996.
- [21] P. S. Tofts, "The distribution of induced currents in magnetic stimulation of the nervous system," *Phys. Med. Biol.*, vol. 35, pp. 1119–1128, 1990.
- [22] B. J. Roth, L. G. Cohen, M. Hallett, W. Friauf, and P. J. Basser, "A theoretical calculation of the electric field induced by magnetic stimulation of a peripheral nerve," *Muscle Nerve*, vol. 13, pp. 734–741, 1990.
- [23] B. J. Roth, J. M. Saypol, M. Hallett, and L. G. Cohen, "A theoretical calculation of the electric field induced in the cortex during magnetic stimulation," *Electroencephalogr. Clin. Neurophysiol.*, vol. 81, pp. 47–56, 1991.
- [24] B. J. Roth, L. G. Cohen, and M. Hallett, "The electric field induced during magnetic stimulation," *Electroencephalogr. Clin. Neurophysiol. (Suppl.)*, vol. 43, pp. 268–278, 1991.
- [25] P. J. Maccabee, V. E. Amassian, L. P. Eberle, A. P. Rudell, R. Q. Cracco, K. S. Lai, and M. Somasundaram, "Measurement of the electric field induced into inhomogeneous volume conductors by magnetic coils: Application to human spinal neurogeometry," *Electroencephalogr. Clin. Neurophysiol.*, vol. 81, pp. 224–237, 1991.
- [26] M. Kobayashi, S. Ueno, and T. Kurokawa, "Importance of soft tissue inhomogeneity in magnetic peripheral nerve stimulation," *Electroencephalogr. Clin. Neurophysiol.*, vol. 105, pp. 406–413, 1997.
- [27] C. R. Johnson, "Computational and numerical methods for bioelectric field problems," *Crit. Rev. Biomed. Eng.*, vol. 25, pp. 1–81, 1997.
- [28] W. Wang and S. R. Eisenberg, "A three-dimensional finite element method for computing magnetically induced currents in tissues," *IEEE Trans. Magn.*, vol. 30, pp. 5015–5023, Nov. 1994.
- [29] R. Liu and S. Ueno, "Calculating the activation function of nerve excitation in inhomogeneous volume conductor during magnetic stimulation using the finite element method," *IEEE Trans. Magn.*, vol. 36, pp. 1796–1799, July 2000.
- [30] G. A. Mouchawar, J. A. Nyenhuis, J. D. Bourland, L. A. Geddes, D. J. Schaefer, and M. E. Riehl, "Magnetic stimulation of excitable tissue: Calculation of induced eddy-currents with a three-dimensional finite-element model," *IEEE Trans. Magn.*, vol. 29, pp. 3355–3357, Nov. 1993.
- [31] G. Cerri, R. De Leo, F. Moglie, and A. Schiavoni, "An accurate 3-D model for magnetic stimulation of the brain cortex," *J. Med. Eng. Technol.*, vol. 19, pp. 7–16, 1995.
- [32] P. J. Basser, J. Mattiello, and D. LeBihan, "Estimation of the effective self-diffusion tensor from the NMR spin echo," *J. Magn. Reson. B*, vol. 103, pp. 247–254, 1994.
- [33] —, "MR diffusion tensor spectroscopy and imaging," *Biophys. J.*, vol. 66, pp. 259–267, 1994.
- [34] D. S. Tuch, V. J. Wedeen, A. M. Dale, J. S. George, and J. W. Belliveau, "Conductivity tensor mapping of the human brain using diffusion tensor MRI," *Proc. Nat. Acad. Sci. USA*, vol. 98, pp. 11 697–11 701, 2001.
- [35] P. C. Miranda, S. Pajevic, C. Pierpoali, M. Hallett, and P. J. Basser, "The distribution of currents induced in the brain by magnetic stimulation: A finite element analysis incorporating DT-MRI-derived conductivity data," presented at the ISMRM-ESMRMB Joint Annual Meeting, Glasgow, Scotland, U.K., 2001.
- [36] R. Plonsey and D. B. Heppner, "Considerations of quasistationarity in electrophysiological systems," *Bull. Math. Biophys.*, vol. 29, pp. 657–664, 1967.
- [37] G. De Mercato and F. J. Garcia Sanchez, "Correlation between low-frequency electric conductivity and permittivity in the diaphysis of bovine femoral bone," *IEEE Trans. Biomed. Eng.*, vol. 39, pp. 523–526, May 1992.
- [38] D. J. Griffiths, *Introduction to Electrodynamics*, 2nd ed. Englewood Cliffs: Prentice-Hall, 1989.
- [39] J. D. Jackson, *Classical Electrodynamics*, 2nd ed. New York: Wiley, 1975.
- [40] S. B. Baumann, D. R. Wozny, S. K. Kelly, and F. M. Meno, "The electrical conductivity of human cerebrospinal fluid at body temperature," *IEEE Trans. Biomed. Eng.*, vol. 44, pp. 220–223, Mar. 1997.
- [41] W. H. J. Freygang and W. M. Landau, "Some relations between resistivity and electrical activity in the cerebral cortex of the cat," *J. Cell. Comp. Physiol.*, vol. 45, pp. 377–392, 1955.
- [42] J. B. Ranck, Jr., "Specific impedance of rabbit cerebral cortex," *Exp. Neurol.*, vol. 7, pp. 144–152, 1963.
- [43] A. van Harrevelde, T. Murphy, and K. W. Nobel, "Specific impedance of rabbit's cortical tissue," *Amer. J. Physiol.*, vol. 205, pp. 203–207, 1963.
- [44] J. B. Ranck, Jr., "Electrical impedance in the subicular area of rats during paradoxical sleep," *Exp. Neurol.*, vol. 16, pp. 416–437, 1966.
- [45] P. N. Robillard and Y. Poussart, "Specific-impedance measurements of brain tissues," *Med. Biol. Eng. Comput.*, vol. 15, pp. 438–445, 1977.
- [46] L. D. Landau, E. M. Lifshitz, and L. P. Pitaevskii, *Electrodynamics of Continuous Media*, 2nd ed. Oxford, U.K.: Butterworth-Heinemann, 1984, vol. 8.
- [47] O. Biro and K. Preis, "On the use of the magnetic vector potential in the finite element analysis of three-dimensional eddy currents," *IEEE Trans. Magn.*, vol. 25, pp. 3145–3159, July 1989.
- [48] H. Eaton, "Electric field induced in a spherical volume conductor from arbitrary coils: Application to magnetic stimulation and MEG," *Med. Biol. Eng. Comput.*, vol. 30, pp. 433–440, 1992.

- [49] W. R. Smythe, *Static and Dynamic Electricity*, 3rd (revised) ed. New York: Taylor & Francis, 1989.
- [50] P. W. Nicholson, "Specific impedance of cerebral white matter," *Exp. Neurol.*, vol. 13, pp. 386–401, 1965.
- [51] J. B. Ranck, Jr. and S. L. BeMent, "The specific impedance of the dorsal columns of cat: An anisotropic medium," *Exp. Neurol.*, vol. 11, pp. 451–463, 1965.
- [52] J. P. Brasil-Neto, L. G. Cohen, M. Panizza, J. Nilsson, B. J. Roth, and M. Hallett, "Optimal focal transcranial magnetic activation of the human motor cortex: Effects of coil orientation, shape of the induced current pulse, and stimulus intensity," *J. Clin. Neurophysiol.*, vol. 9, pp. 132–136, 1992.
- [53] V. Di Lazzaro, A. Oliviero, P. Profice, E. Saturno, F. Pilato, A. Insola, P. Mazzone, P. Tonali, and J. C. Rothwell, "Comparison of descending volleys evoked by transcranial magnetic and electric stimulation in conscious humans," *Electroencephalogr. Clin. Neurophysiol.*, vol. 109, pp. 397–401, 1998.



Pedro C. Miranda received the B.Sc. and Ph.D. degrees in physics from the University of Sussex, Sussex, UK in 1981 and 1987, respectively, and the M.Sc. degree in computer science from University College, London, U.K., in 1992.

He was a Research Fellow at the University of Sussex, Sussex, U.K., from 1985 to 1986, and at St. George's Hospital Medical School, London, U.K., from 1987 to 1991. He is currently an Assistant Professor in the Physics Department of the University of Lisbon, Lisbon, Portugal. His research interests

include magnetic stimulation of excitable tissues, bioelectromagnetism, and magnetic resonance imaging.



Mark Hallett received the M.D. degree from Harvard University, Cambridge, MA, in 1969.

He trained in neurology at Massachusetts General Hospital. He had fellowships in neurophysiology at the National Institutes of Health and at the Institute of Psychiatry in London, U.K. From 1976 to 1984, he was the Chief of the Clinical Neurophysiology Laboratory at the Brigham and Women's Hospital, Boston, MA, and Associate Professor of Neurology at Harvard Medical School. Since 1984, he has been at the National Institute of Neurological Disorders and Stroke where he serves as Chief of the Human Motor Control Section and pursues research on the physiology of human movement disorders and other problems of motor control. He also served as Clinical Director of NINDS until July 2000.

Dr. Hallett is past President of the American Association of Electrodiagnostic Medicine and the Movement Disorder Society. He is currently Vice-President of the American Academy of Neurology, and Editor-in-Chief of *Clinical Neurophysiology*.



Peter J. Basser received the A.B., S.M., and Ph.D. degrees from Harvard University, Cambridge, MA, in 1980, 1982, and 1986, respectively.

In 1986, he received a Staff Fellowship appointment in the Biomedical Engineering and Instrumentation Program (BEIB) of the National Institutes of Health (NIH), Bethesda, MD, and in 1997, became Chief of the Section on Tissue Biophysics and Biomimetics within the National Institute of Child Health and Human Development (NICHD) and Senior Investigator. His research

focuses primarily on elucidating relationships between tissue structure and function. He has contributed to the understanding of the mechanisms of action of electromagnetic fields on excitable tissues (magnetic stimulation), measuring and characterizing diffusive transport of water in tissues using magnetic resonance imaging methods (DT-MRI), and explaining the functional properties of extracellular matrices (such as cartilage) in terms of the osmotic properties of its constituents.